Quaternary Research 75 (2011) 417–429

Contents lists available at ScienceDirect

Quaternary Research

journal homepage: www.elsevier.com/locate/yqres

Is the East Antarctic ice sheet stable?

Katherine Pingree [a], Max Lurie [a], Terence Hughes [a,b,*]

[a] Department of Earth Sciences, University of Maine, Orono, ME 04469-5790, USA
[b] Climate Change Institute, University of Maine, Orono, ME 04469-5790, USA

ARTICLE INFO

Article history:
Received 7 October 2010
Available online 13 January 2011

Keywords:
East Antarctic ice sheet
Ice streams
Ice shelves
Rising sea level
Climate change

ABSTRACT

The Greenland and East and West Antarctic ice sheets are assessed as being the source of ice that produced an Eemian sea level 6 m higher than present sea level. The most probable source is total collapse of the West Antarctic Ice Sheet accompanied by partial collapse of the adjacent sector of the East Antarctic Ice Sheet in direct contact with the West Antarctic Ice Sheet. This conclusion is reached by applying a simple formula relating the "floating fraction" of ice along flowlines to ice height above the bed. Increasing the floating fraction lowered ice elevations enough to contribute up to 4.7 m to global sea level. Adding 3.3 m resulting from total collapse of the West Antarctic Ice Sheet accounts for the higher Eemian sea level. Partial gravitational collapse that produced the present ice drainage system of Amery Ice Shelf contributes 2.3 m to global sea level. These results cast doubt on the presumed stability of the East Antarctic Ice Sheet, but destabilizing mechanisms remain largely unknown. Possibilities include glacial surges and marine instabilities at the respective head and foot of ice streams.

Introduction

An enduring mystery of the Quaternary ice age is the source of the high Eemian sea level, 6 m higher than present sea level at the last interglacial maximum and possibly even higher sea levels in the more distant past. Hollin (1962, 1972) linked these higher sea levels to instabilities in the Antarctic Ice Sheet, which today impounds ice equivalent to some 70 m of sea level. Mercer (1968, 1970) ascribed the higher Eemian sea level to collapse of an Eemian West Antarctic Ice Sheet (WAIS), which presumably had a size comparable to the WAIS today and was inherently unstable, being a largely marine ice sheet grounded below sea level. However, Bamber et al. (2009) have shown that collapse of today's WAIS would cause sea level to rise by only 3.3 m. This leaves only the East Antarctic Ice Sheet (EAIS) and the Greenland Ice Sheet (GIS) as sources for higher Quaternary sea levels. Today, the GIS impounds ice equivalent to about 7 m of sea level. Its bed is frozen under the high central dome and has been frozen for some 130,000 years (Alley et al., 1997; Mayewski et al., 1997), so the GIS was probably largely intact during the Eemian. Most Greenland ice today is discharged by ice streams that become outlet glaciers confined in narrow fjords. Pfeffer et al. (2008) have shown that these restrictive fjord boundaries prevent large-scale collapse of the GIS by way of increased surge-like discharge from ice streams, such as has begun in recent years (Thomas et al., 2009). These increases have been attributed to surface meltwater reaching the bed (Van der Wal et al., 2008) and warmer ocean water entering the fjords (Christoffersen et al., 2008; Holland et al., 2008). Modeling studies suggest these surges may last only a few years (Thomas, 2004). Even a worst-case scenario provides only a 2 m rise in sea level and leaves the GIS largely intact (Hughes, 2004). We seem to be left with the EAIS as the most probable source of Quaternary sea levels 6 m or more higher than at present, both in the past and in the future. Here we examine that prospect.

Figure 1 shows the Antarctic Ice Sheet today, including the boundaries of major ice-drainage basins that supply major ice streams and that provide case-studies for assessing stability of the ice sheet as a whole. Note that Ross Ice Shelf and Ronne-Filchner Ice Shelf occupy the respective Ross Sea and Weddell Sea marine embayments. These embayments were occupied by an expanded WAIS at the last glacial maximum that was triple the size of the WAIS today (Denton and Hughes, 2002). Gravitational collapse of these sectors began in earnest during the Holocene, after rising sea level from collapsing Northern Hemisphere ice sheets had largely ceased (Hall et al., 2004). Hughes (1975) proposed two mechanisms for WAIS collapse, past and future. The first was the glacial surge mechanism proposed by Robin and Weertman (1973), but applied to WAIS ice streams. Bindschadler (1997) gave evidence for this mechanism being active today in ice streams entering Ross Ice Shelf. In this mechanism, ice actively lowering at the heads of surging ice streams eventually causes ice-shelf grounding lines to reactively retreat. The second was the marine instability mechanism developed by Weertman (1974) and later applied to the Ross sector by Thomas and Bentley (1978), and then to all WAIS sectors by Stuiver et al. (1981). In this mechanism, actively retreating ice-shelf grounding lines drove reactive collapse of interior ice. In both mechanisms, ice thins as a result of ice-bed

* Corresponding author. Climate Change Institute, University of Maine, Orono, ME 04469-5790, USA.
E-mail address: terry.hughes@maine.edu (T. Hughes).

0033-5894/$ – see front matter © 2011 University of Washington. Published by Elsevier Inc. All rights reserved.
doi:10.1016/j.yqres.2010.12.001

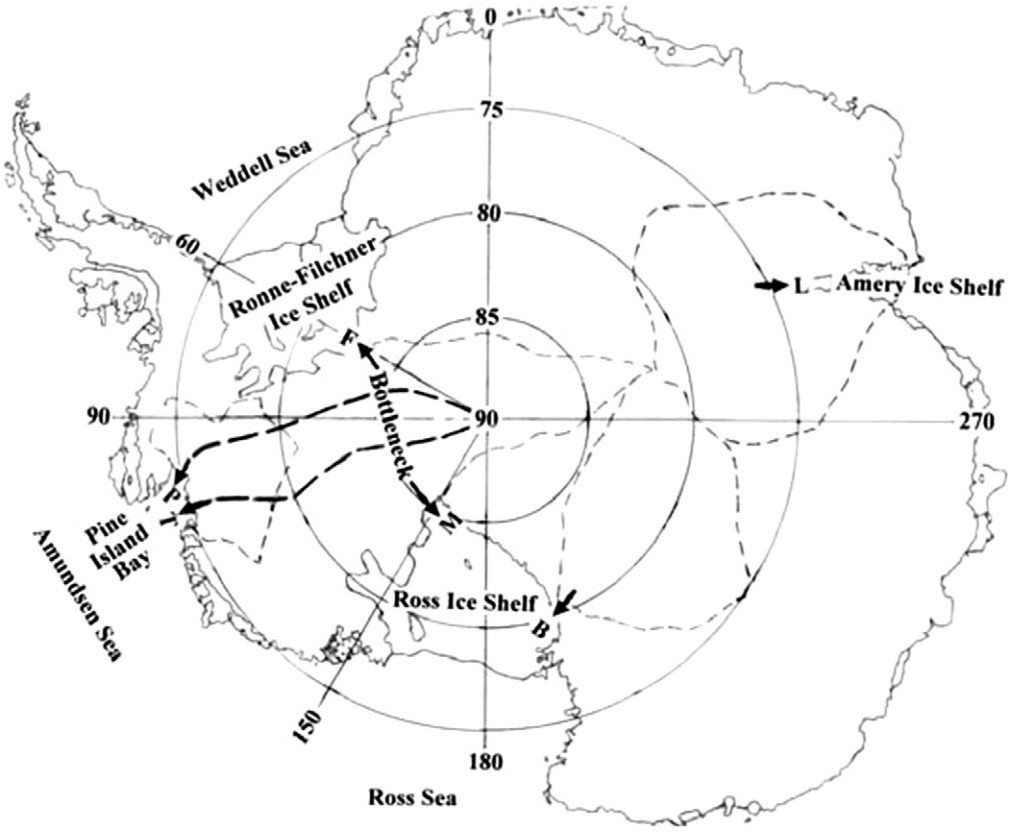

Figure 1. Geographical setting of the Bottleneck. Major ice streams shown by arrows are Foundation Ice Stream (F), Mercer Ice Stream (M), Pine Island Glacier (P), Thwaites Glacier (T), Byrd Glacier (B), and Lambert Glacier (L). Heavy dashed lines show future ice-stream retreat routes. Light dashed lines enclose present ice drainage basins.

uncoupling, either beneath ice streams that supply the ice shelves or beneath confined and pinned ice shelves in marine embayments. The glacial surge mechanism (Kamb et al., 1985) applies to both marine and terrestrial portions of the WAIS and the EAIS. The marine instability mechanism only applies to marine parts of these ice sheets (Schoof, 2007). This is important in assessing stability of the EAIS.

The following sections provide a hypothesis for studying ice-sheet stability, applications to possible former and future partial collapse in two EAIS ice drainage systems, and a discussion of how these systems can be studied more fully.

A hypothesis to measure stability of ice sheets

The hypothesis applied to measure stability of the EAIS is based on three postulates. (1) Ice height above the bed is controlled by the strength of ice-bed coupling, reducing ice thickness by some 90% when coupling vanishes. (2) Ice-bed coupling vanishes along ice streams that end as floating ice shelves and drain up to 90% of an ice sheet. (3) Because of (1) and (2), ice sheets can rapidly collapse and disintegrate, thereby removing ice sheets from Earth's climate system and forcing abrupt climate change. This hypothesis has been assessed by Hughes (2009a). Here we deal with (1) and (2), using linear ice flow for simplicity, prior to our EAIS applications.

Consider a longitudinal force balance for linear sheet flow. Approximate the bed by an up-down staircase, with vertical ice columns having height h_I and horizontal basal area A_z on steps, so ice thickness gradient $\Delta h_I/\Delta x$ along flow equals ice surface slope $\Delta h/\Delta x$. Changes in bed slope take place between ice columns. Ice motion is caused by horizontal gravitational driving force $F_G = \overline{P}_I A_x$ for average ice pressure $\overline{P}_I = \frac{1}{2}P_I = \frac{1}{2}\rho_I\, g\, h_I$ acting on transverse vertical area $A_x = w_I\, h_I$, where P_I is basal ice pressure, ρ_I is ice density, g is gravity acceleration, h_I is ice thickness, and w_I is flowband width at horizontal distance x from the grounded ice margin. Resisting horizontal ice motion is force $F_R = (\overline{P}_I - \Delta\overline{P}_I)(A_x - \Delta A_x) + \tau_O A_z$, where $\Delta\overline{P}_I = \frac{1}{2}\rho_I\, g\, \Delta h_I$ and $\Delta A_x = w_I\, \Delta h_I$ due to change Δh_I of ice elevation in Δx, and τ_O is the basal shear stress in basal area $A_z = w_I\ \Delta x$ normal to the vertical z direction. Setting $F_G = F_R$ gives, to a first approximation, for surface slope α at x as Δx shrinks to zero:

$$\tau_O = \rho_I g h_I \alpha = P_I \alpha \tag{1}$$

In linear unconfined shelf flow, a first approximation balances gravitational force $F_G = (\overline{P}_I A_x)_I = (\frac{1}{2}\rho_I\, g\, h_I)\ (w_I\, h_I)$ against resisting force $F_R = (\overline{P}_W A_x)_W + (\sigma_T A_x)_I = (\frac{1}{2}\rho_W\, g\, h_W)(w_I\, h_W) + \sigma_T\, w_I\, h_I$. Here $\overline{P}_I$ and $\overline{P}_W$ are average ice and water pressures at the vertical front of the ice shelf, ρ_W is water density, h_W is water depth at the base of floating ice, where water pressure $P_W = \rho_W g h_W = P_I = \rho_I g h_I$ to satisfy the buoyancy requirement. Longitudinal tensile stress σ_T acts on transverse vertical cross-sectional area $A_x = w_I\, h_I$. Setting $F_G = F_R$ and solving for σ_T using $\rho_W h_W = \rho_I h_I$ for buoyancy:

$$\sigma_T = {}^1\!/_2 \rho_I g\, h_I - \rho_W g\, h_W (h_W / h_I) = \overline{P}_I (1 - \rho_I / \rho_W) \tag{2}$$

Taking w_I constant, F_G and F_R use triangular areas $\overline{P}_I h_I$ for ice and $\overline{P}_W h_W$ for water. Setting $F_G = F_R$ to obtain Equations (1) and (2) therefore employs a geometrical force balance in the flow direction (Hughes, 2009b). The same expressions for τ_O and σ_T are obtained by integrating the equilibrium/momentum equations for linear sheet flow (Nye, 1952) and linear shelf flow (Weertman, 1957a), respectively.

Representative EAIS values are $h_I \approx 2$ km and $\alpha \approx 0.005$, giving $\tau_O \approx 100$ kPa using Equation (1). Taking $h_I = 2$ km and $\rho_I/\rho_W \approx 0.9$ gives $\sigma_T \approx 1000$ kPa using Equation (2). The viscoplastic "yield stress" of ice σ_O requires that $\sigma_O \approx \tau_O \approx \sigma_T \approx 100$ kPa (Paterson, 1994). Therefore grounded ice 2 km thick thins to floating ice about 200 m thick when ice-bed coupling is totally removed, as is observed at the

https://doi.org/10.1016/j.yqres.2010.12.001 Published online by Cambridge University Press

calving fronts of ice shelves (Drewry, 1983). This satisfies postulate (1). That this thinning occurs along ice streams, converting the high convex profile of sheet flow into the low concave profile of stream flow to become the nearly flat profile of shelf flow, satisfies postulate (2). Equations (1) and (2) are the respective sheet flow and shelf flow end members for continuous transitions from fully grounded sheet flow to fully floating shelf flow. The transition is made by specifying an increasing "floating fraction" ϕ downstream for ice in stream flow.

Equation (2) applies at the grounding line of a freely floating ice shelf, even though water does not contact a vertical ice face as it does at the calving front. This is because the buoyancy requirement $P_I = P_W$ is satisfied at both locations and at all locations in between (Hughes, 2009b). Thomas (1973a,b) modified Equation (2) to include back-stress σ_B when the ice shelf is in a confined embayment and/or is pinned to the sea floor, producing ice rumples and ice rises on the ice surface. At the ice-shelf grounding line with an ice stream where $x = 0$, $\sigma_T = (\sigma_T)_O$, and $h_I = h_O$:

$$\sigma_T = R[\tfrac{1}{2}\rho_I g\, h_O(1-\rho_I/\rho_W)-\sigma_B] \tag{3}$$

Here $R = \left[1 + (\dot{\varepsilon}_{yy}/\dot{\varepsilon}_{xx}) + (\dot{\varepsilon}_{yy}/\dot{\varepsilon}_{xx})^2 + (\dot{\varepsilon}_{xy}/\dot{\varepsilon}_{xx})^2 + (\dot{\varepsilon}_{xz}/\dot{\varepsilon}_{xx})^2\right]^{1/2}$ takes account of the geometry of the ice shelf by including transverse strain rates $\dot{\varepsilon}_{yy}$, side shear strain rates $\dot{\varepsilon}_{xy}$ alongside the embayment and ice rises, and basal shear strain rates $\dot{\varepsilon}_{xz}$ at ice rumples (Hughes 1998, page 170). Ice flows around firm basal pinning to produce surface ice rises, and scrapes across weaker basal pinning to produce surface ice rumples. Solving Equation (3) for h_O:

$$h_O = \frac{2(\sigma_T + R\sigma_B)}{R\rho_I g(1-\rho_I/\rho_W)} \tag{4}$$

Note that h_O increases as ice-shelf buttressing quantified by σ_B increases. Thomas (1973a,b) shows how σ_B is calculated for McDonald Ice Rumples on Brunt Ice Shelf in East Antarctica.

By definition, floating fraction ϕ of ice at any location along x is the ratio of area A_F where ice is uncoupled from the bed and therefore "floating" to basal area A_I. An assumption is that, for an ice column of base A_I and height h_I, area A_F supports floating height h_F and grounded area A_I–A_F supports grounded height h_I–h_F so that:

$$\phi = A_F/A_I = h_F/h_I \tag{5}$$

Total coupling in sheet flow requires $A_F = 0$ so that $\phi = 0$ and $h_F = 0$ for a grounded ice sheet ending on land (Nye, 1952). Total uncoupling in shelf flow requires $A_F = A_I$ so that $\phi = 1$ and $h_F = h_I$ for a freely floating ice shelf (Weertman, 1957a).

The appendix shows how the longitudinal force balance provides a first-order approximation to Equation (5) given by:

$$\phi \approx h_O/h_I \tag{6}$$

Here h_O substitutes for h_F in Equation (5). Equation (5) allows a frozen bed for which $\phi = 0$, but Equation (6) requires a degree of hydrological continuity all along the flowline because $\phi > 0$ when $h_O > 0$. However, subglacial lakes are widespread in East Antarctica (Smith et al., 2009), as Bell (2006) noted, so Equation (6) is a reasonable first-approximation to Equation (5). Note that $\phi > 0$ when $h_O > 0$ applies only for a marine ice sheet grounded below sea level. If the ice sheet ends on land, $\phi = h_O = 0$ and the ice sheet is grounded everywhere. This is a limitation of the approximation $\phi \approx h_O/h_I$ in Equation (6). It results from applying a longitudinal force balance while ignoring the mass balance. Including the mass balance allows regions where $\phi = 0$ even when $h_O > 0$. As an ice shelf becomes increasingly confined and pinned, a greater gravitational driving force $(F_G)_O = (\overline{P}_I w_I h_I)_O = \tfrac{1}{2}\rho_I g w_I h_O^2$ at $x = 0$ is required to "push" the ice shelf forward. Therefore h_O increases as an ice shelf becomes increasingly confined and pinned, as shown by Equation (4).

Although Equation (6) is remarkably simple, it is quite robust, applying to both flowbands and flowlines. Equation (6) is derived for flowbands using a geometrical force balance in the direction of ice flow (Hughes, 2009b). Our appendix provides the flowline derivation. In the flowband derivation, basal shear stress τ_O, side shear stress τ_S, upslope tensile stress σ_T, and downslope compressive stress σ_C are all derived locally for h_I at distance x from the ungrounding line where $x = 0$ and $h_I = h_O$, and all depend on the local value of floating fraction ϕ of ice. Flowband applications are most useful in ice streams where τ_S is important. Flowline applications apply down the centerline of ice streams where $\tau_S = 0$ and the effects of side drag are incorporated into τ_O for basal drag (Hofstede, 2008).

Possible former collapse of the amery ice drainage system

Figure 1 shows the Amery ice drainage system that supplies Amery Ice Shelf. The main supplier is Lambert Glacier, but smaller outlet glaciers also supply ice. Figure 2 shows the surface and bed topography for this system using BEDMAP data. Ice elevation contours bow deeply inward, suggesting massive gravitational collapse of ice at some time in the past. Contours bow inward when the ice surface lowers substantially over this region. Keeping first-order limitations in mind, Figure 2 shows five flowlines from the East Antarctic ice divide to the marine ice margin where ice becomes afloat on the Antarctic continental shelf facing the Indian Ocean, before our postulated gravitational collapse lowered the ice surface and produced the Amery ice drainage system. Ice elevation contours at 250 m intervals before the collapse of the system are shown as straight lines that connect with present-day uncollapsed ice elevations. Flowlines 1 through 5 are approximately normal to these straight contour lines. This approximation is acceptable for a first-order study. Four present-day flowlines in the Amery ice drainage system are numbered 1 through 4. All converge at the head of Amery Ice Shelf, which apparently begins at a fjord headwall that is not resolved by BEDMAP data (see Craven et al., 2009).

Figure 3 shows surface and bed profiles along the five "pre-collapse" flowlines in Figure 2, the resulting ice thickness profiles, and values of ϕ delivered by Equation (6). Ice flows above a bed having variable topography, along which τ_O varies (with $\tau_O = 0$ at $x = 0$ where $h_I = h_O$). All profiles are convex where $\phi \approx 0.2$, except for a concave portion <100 km long along which ϕ climbs rapidly from about 0.2 to 1.0 at the ungrounding line. These concave portions represent ice-bed uncoupling as grounded ice increasingly becomes afloat. A high rugged bed near the ice margin in flowline four makes ϕ vary erratically in this region. For uniformity, all flowlines end in water 500 m deep, giving $h_O = 550$ m in Equation (6) as ice becomes afloat at $x = 0$. The value $\phi \approx 0.2$ for sheet flow allows ice elevations h at the East Antarctic ice divide to match present-day elevations.

Figure 4 shows surface and bed profiles, the resulting ice thickness profiles, and the ϕ variations obtained from Equation (6) along each of the four "post-collapse" present-day flowlines in Figure 2. Ice surfaces are convex where $\phi \approx 0.4 \pm 0.2$, but ϕ increases rapidly to 1.0 at the ungrounding line in about the last 300 km, with a sharp dip toward 0.2 at a probable fjord headwall ($x \approx 30$ km), allowing it to partly "dam" inland basal water. The ice surface loses much of its convex profile but it does not become the concave profile of stream flow, partly owing to rugged bed topography but mainly because these are flowlines for strongly converging sheet flow, not for linear stream flow (see Fig. 5.10 in Hughes, 1998). The fjord headwall is not resolved by BEDMAP but it can be inferred from the grounding line of Amery Ice Shelf in water 2500 m deep (Craven et al., 2009). Equation (6) is unsuited for rugged bed topography, especially for determining h_O where ungrounding occurs at a fjord headwall. We took $h_O = 1000$ m to prevent $\phi > 1.0$ along the four flowlines in Figure 4. The ice surface

https://doi.org/10.1016/j.yqres.2010.12.001 Published online by Cambridge University Press

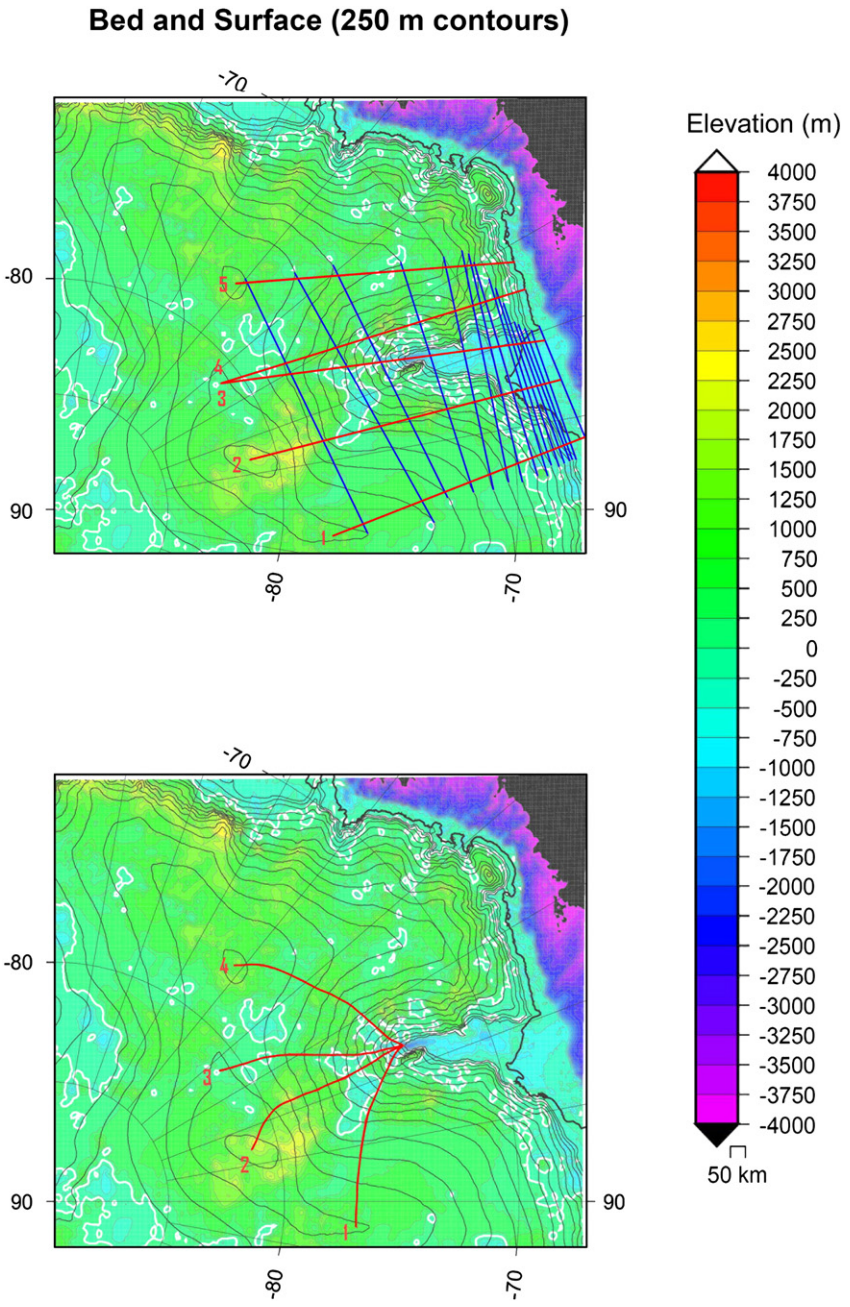

Figure 2. Surface and bed topography of the Amery Ice Shelf ice drainage system from BEDMAP data contoured at 250 m intervals. The color bar is divided into 250 m intervals of bed topography above (positive) and below (negative) sea level. White contour lines show sea level in the map plane. Five flowlines are shown approximately normal to postulated former surface ice contours before the drainage basin formed (top). Four flowlines are shown normal to present-day surface ice contours (bottom).

has lowered 3000 m at the ungrounding line from the former ice surface in Figure 2.

Possible future collapse of the "bottleneck" ice drainage system

As shown in Figure 1, the so-called "bottleneck" is the gap in the Transantarctic Mountains through which the EAIS flows into the WAIS. It extends from 60°W to 150°W at 84°S, a length of nearly 1000 km. At the last glacial maximum (LGM), this junction extended along the entire length of the Transantarctic Mountains, some 4000 km long (Denton and Hughes, 2002). Now the remaining grounded West Antarctic Ice Sheet acts like a "cork in the bottle" that keeps East Antarctic ice from pouring through the bottleneck. This gap is the "neck" in the East Antarctic "bottle." East Antarctic ice entering the bottleneck is diverted by the Thiel Mountains massif into Foundation Ice Stream, which supplies Ronne–Filchner Ice Shelf, and Mercer Ice Stream, which supplies Ross Ice Shelf. Holocene collapse of the Ross and Weddell sectors of the WAIS may have produced these ice shelves (see Stuiver et al., 1981). Collapse nearly to sea level greatly increased the surface slope of EAIS ice streams passing through fjords in the Transantarctic Mountains. The largest fjord is occupied by Byrd Glacier, shown in Figure 1. Today the Ross Ice Shelf grounding line is halfway up the fjord, and polished bedrock along the fjord walls require a former ice surface at least 1000 m higher than the present ice surface. The steepened surface resulted in faster ice discharge rates that have downdrawn East Antarctic ice and produced the enormous ice drainage system shown in Figure 1, even though Byrd Glacier occupies a fjord only 25 km wide at its narrowest point,

https://doi.org/10.1016/j.yqres.2010.12.001 Published online by Cambridge University Press

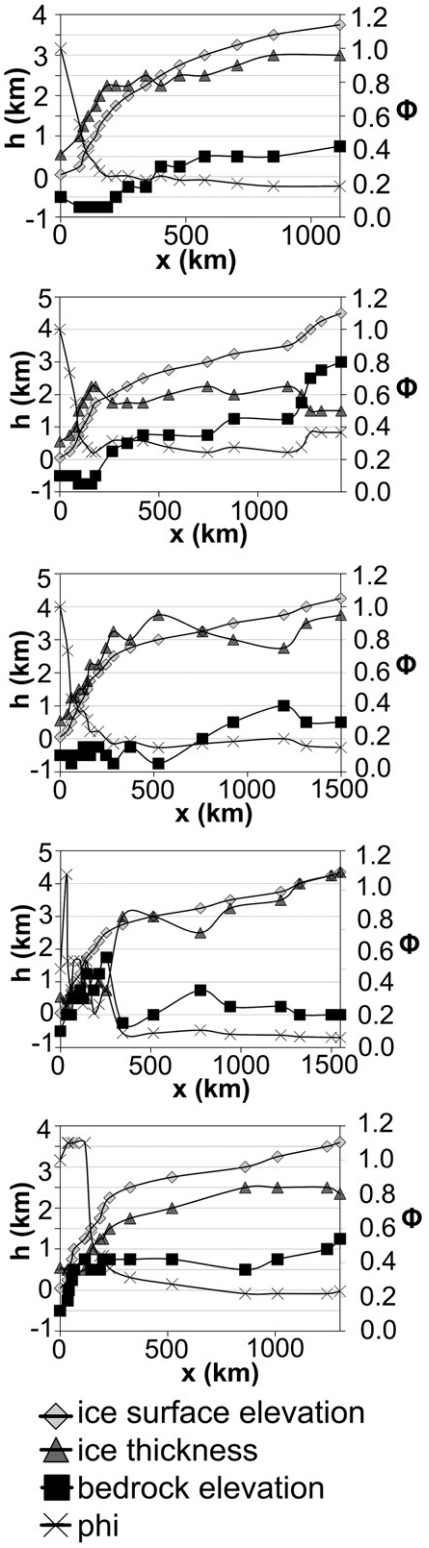

Figure 3. Surface, bed, and ice thickness profiles, and ϕ variations from Eq. (6), are plotted along "pre-collapse" flowlines 1 through 5 in Fig. 2 (top).

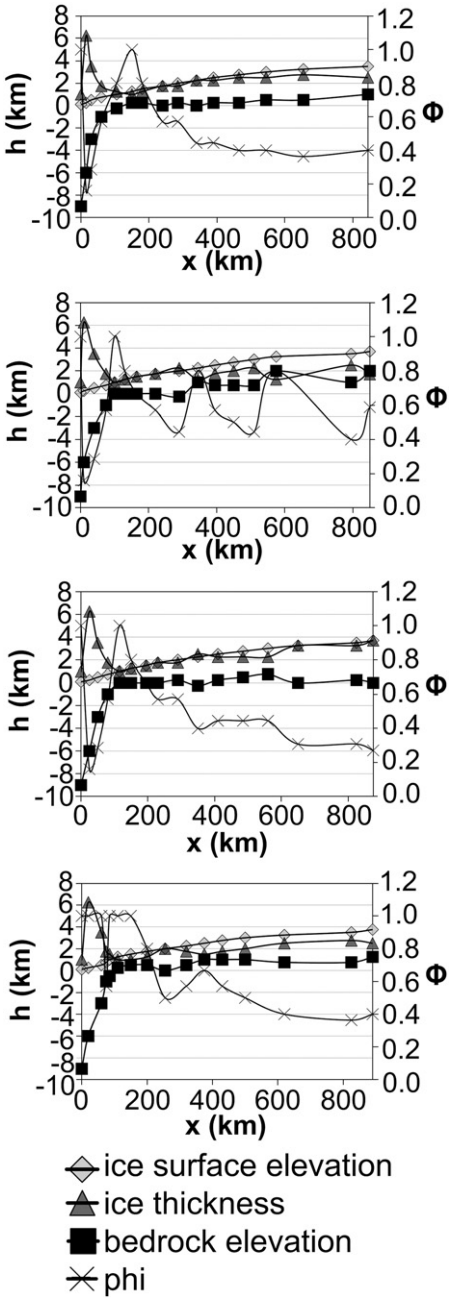

Figure 4. Surface, bed, and ice thickness profiles, and ϕ variations from Eq. (6), are plotted along "post-collapse" flowlines 1 through 4 in Fig. 2 (bottom).

and ice only 1200 m thick crosses the high fjord headwall (Reusch and Hughes, 2003). If the remaining WAIS were to collapse nearly to sea level, a similarly steep surface slope would develop in the bottleneck on both sides of Thiel Mountains. How much East Antarctic ice could be downdrawn in this case? That will now be considered.

Whether Holocene collapse of the WAIS is ongoing today remains an unanswered question, despite nearly four decades of field activities directed at this goal (eg., Hughes, 1973; Alley and Bindschadler, 2001; Joughin et al., 2009). Figure 1 shows the area of East Antarctic ice passing through the bottleneck today. It is smaller than the areas of East Antarctic ice supplying Amery Ice Shelf and Byrd Glacier, but it could enlarge considerably if the WAIS were to collapse to sea level. WAIS collapse has already occurred in the sectors facing the Weddell Sea and the Ross Sea. Further collapse in these sectors would have to overcome buttressing by the large Ronne–Filchner and Ross ice shelves now occupying these embayments. However, the sector facing the Amundsen Sea is not buttressed by large ice shelves, and an ice-free polynya exists in Pine Island Bay, which may have formed during partial Holocene collapse of the WAIS in this sector (Kellogg and Kellogg, 1987). The two fastest West Antarctic ice streams, Pine Island Glacier and Thwaites Glacier, enter Pine Island Bay today and

https://doi.org/10.1016/j.yqres.2010.12.001 Published online by Cambridge University Press

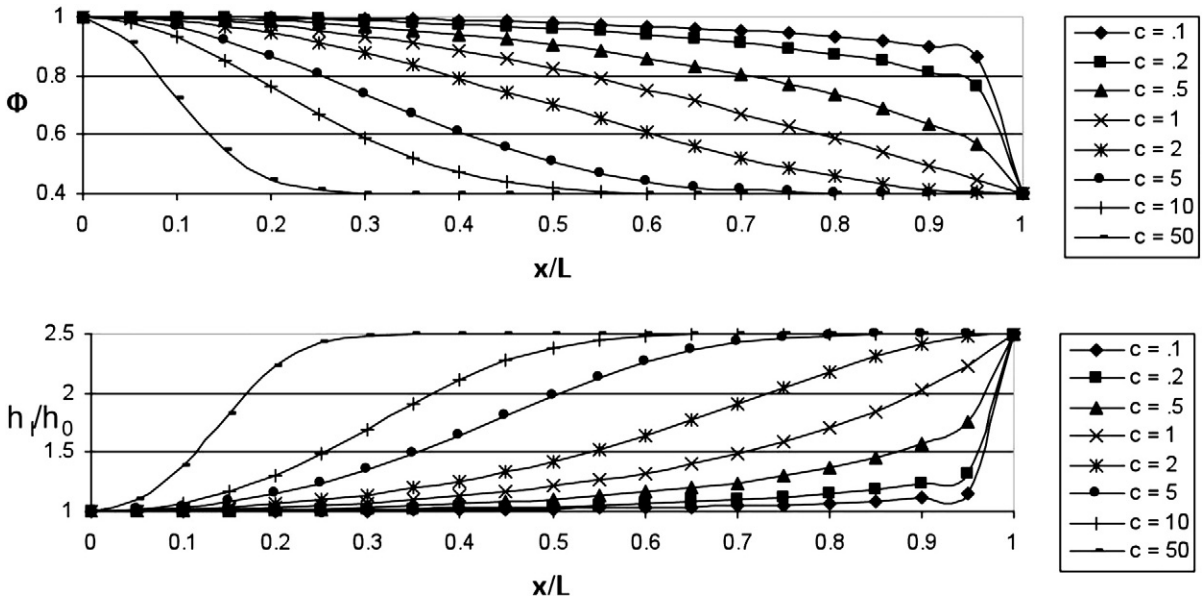

Figure 5. Gravitational collapse of a marine ice sheet on a horizontal bed as c decreases from 50 to 0.1 in Eq. (7), using Eq. (6), due to the progressive ice-bed uncoupling over time. Top: upstream migration of floating fraction ϕ of ice from the ungrounding line. Bottom: normalized surface lowering h_l/h_O along the normalized flowline length x/L.

drain about one-third of the remaining marine portions of the WAIS, see Figure 1 (Joughin et al., 2009). For these reasons Pine Island Bay has been called "the weak underbelly of the WAIS" (Hughes, 1981). With that caution, we propose a scenario for total WAIS collapse similar to that modeled by Stuiver et al. (1981).

Assume that Pine Island Bay becomes a marine embayment of the Amundsen Sea as large as the Weddell and Ross embayments are today. This could result from either or both of the two mechanisms proposed by Hughes (1975), both acting on Pine Island and Thwaites glaciers, the glacial surge mechanism of Robin and Weertman (1973) at their heads and the marine instability mechanism of Weertman (1974) at their ungrounding lines. Then Pine Island and Thwaites glaciers would retreat into West Antarctica along the heavy dashed lines in Figure 1, which follow subglacial basins on opposite sides of the subglacial highlands that contain numerous nunataks from the Thiel Mountains to the Whitmore Mountains. In the bottleneck they would merge with Foundation Ice Stream and Mercer Ice Stream, respectively, producing two giant ice streams that would rapidly downdraw East Antarctic ice due to their steep surface slopes in the bottleneck. This would be similar to East Antarctic ice downdrawn by Byrd Glacier, but on a much larger scale. Contributing to this downdraw would be Institute Ice Stream and Support Force Glacier, both of which drain East Antarctic ice passing through the bottleneck, and enter Ronne–Filchner Ice Shelf.

Gravitational collapse of East Antarctic ice through the bottleneck is accomplished by having ϕ vary along flow according to an ad hoc formula that generates the full spectrum of flowline profiles from convex sheet flow through concave stream flow to flat shelf flow:

$$\phi = \phi_L + (1-\phi_L)\, cos^c(\pi x / 2L) \qquad (7)$$

where $x=0$ at the grounding line, $x=L$ at the ice divide for flowlines of length L, and exponent c varies over the range from $c\to 0$ for pure shelf flow, giving $\phi\to 1$, to $c\to\infty$ for pure sheet flow, giving $\phi\to\phi_L$, for all values of $0\le x\le L$. Figure 5 plots Equation (7) in the top panel and Equation (6) using ϕ obtained from Equation (7) in the bottom panel, both for $0.1\le c\le 50$. The concave profile of stream flow lengthens as c decreases. Concave profiles for stream flow become convex for sheet flow as $x\to$ L when $c>2$.

Figure 6 shows four flowlines from Dome Argus in East Antarctica through the bottleneck into West Antarctica. One flowline separates, with Flowline 1 entering Mercer Ice Stream by way of Reedy Glacier and Flowline 2 entering Institute Ice Stream. Flowlines 3 and 4 both enter Foundation Ice Stream. Flowline 5 enters Support Force Glacier.

In Figure 7, ϕ values today are calculated using Equation (6) and h_I values obtained from present-day surface and bed profiles along each of the five flowlines (left-side panels), whereas collapsing ice elevations h in the future are calculated along the flowlines from bed topography and ice thicknesses h_I obtained from Equation (6) when ϕ is obtained from Equation (7) for $c=2$ during gravitational collapse (center panels) and for $c=0.1$ when gravitational collapse is nearly complete (right-side panels). These plots are shown in five stacked panels for flowlines 1 through 5 from top to bottom in Figure 7. Values of h_O in Equation (6) are specified where flowlines 1 through 5 become afloat at present-day ungrounding lines near the bottleneck. For simplicity, these grounding lines remain fixed as upslope ice thins. In any case, bedrock sills along the Transantarctic Mountains would hamper grounding-line retreat.

Panel 1 in Figure 7 shows gravitational collapse along flowline 1 that enters Mercer Ice Stream. Today, ϕ decreases from 1.0 to about 0.2 in the first 600 km from the ungrounding line, where $h_O=550$ m at $x=0$. Except for the concave ice stream, the flowline surface is convex and climbs steadily for $\phi\approx 0.2$. During gravitational collapse, when $c=2$ in Equation (7), an ice dome develops over subglacial highlands centered around $x=350$ km. Therefore ice will flow around a local ice dome over these highlands. This ice dome remains as collapse goes to completion at $c=0.1$ and surrounding ice continues to lower by 500 m above the marine subglacial basin where ice-bed uncoupling is nearly complete ($\phi>0.9$).

Panel 2 in Figure 7 shows gravitational collapse along flowline 2 that enters Institute Ice Stream. Today, ϕ decreases in a jerky manner from $\phi=1.0$ at $x=0$ to $\phi\approx 0.5$ as $x\to L$, indicating that ice-bed coupling is highly variable along x based to some extent on variable bed topography with $h_O=1512$ m at $x=0$. A smooth decrease of ϕ along x provided by $c=2$ in Equation (7) during gravitational collapse produces an ice dome above the same subglacial highlands as for flowline 1 because these two flowlines merge in this region. This dome remains when gravitational collapse is nearly complete at $c=0.1$, with $\phi\approx 0.95$ over the subglacial basin between the subglacial highlands and Dome Argus.

Panel 3 in Figure 7 shows gravitational collapse along flowline 3 that enters Foundation Ice Stream today. Unlike flowlines 1 and 2,

https://doi.org/10.1016/j.yqres.2010.12.001 Published online by Cambridge University Press

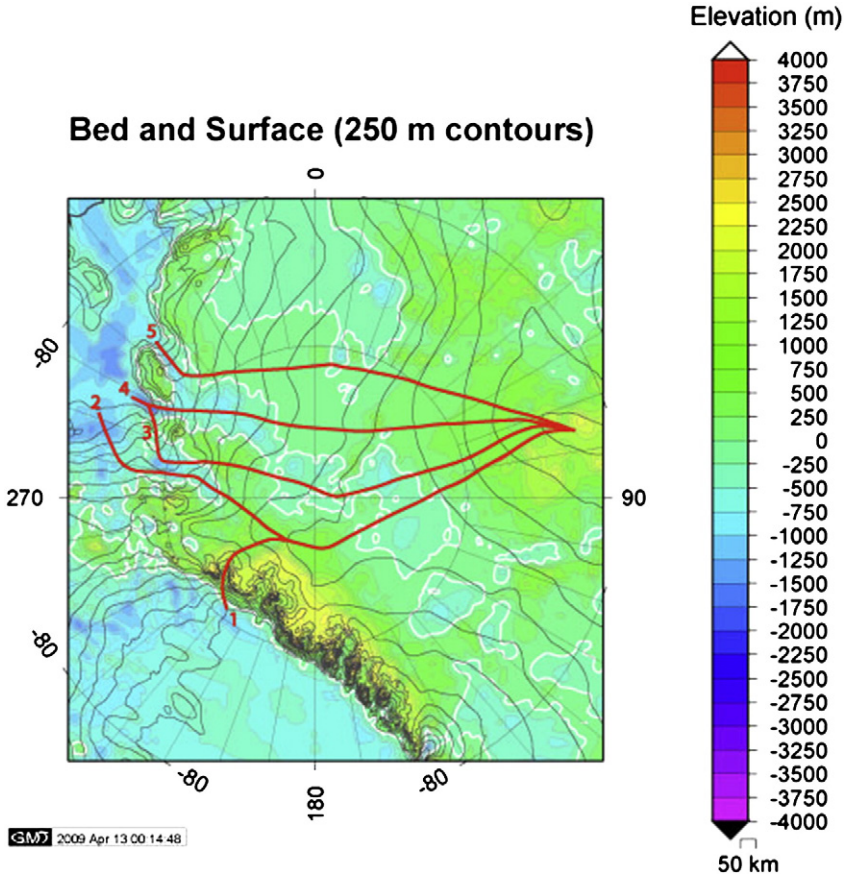

Figure 6. Surface and bed topography of the Bottleneck ice drainage system from BEDMAP data contoured at 250 m intervals. Five flowlines are shown normal to surface ice contours at the present time. The color bar is divided into 250 m intervals of bed topography above (positive) and below (negative) sea level. White contour lines show sea level in the map plane.

flowline 3 passes over a bed that is close to sea level along most of its length except under the ice stream, for which $h_O = 1100$ m at $x = 0$, and when crossing Gamburtsev Subglacial Mountains under Dome Argus as $x \rightarrow L$. The concave ice stream surface, modified by bed topography, is 500 km long, over which ϕ decreases from 1.0 at $x = 0$ to about 0.4, and remains close to 0.4 from there to Dome Argus. During gravitational collapse, the concave ice surface moves towards Dome Argus for $c = 2$ in Equation (7), and images bed topography. When gravitational collapse is nearly complete for $c = 0.1$, the concave surface modified by bed topography extends all the way to Dome Argus and ice thickness is nearly constant all along x.

Panel 4 in Figure 7 shows gravitational collapse along flowline 4, which enters Foundation Ice Stream today with $h_O = 1100$ m at $x = 0$ and a bed below sea level until $x = 450$ km and only 100 m above sea level until $x = 700$ km, before the bed climbs toward the Gamburtsev Subglacial Mountains under Dome Argus. A concave ice-stream surface extends to $x = 150$ km at a fjord headwall, which causes a jog in ϕ as it decreases from 1.0 at $x = 0$ to 0.45 at $x = 300$ km, before remaining close to 0.4 on to Dome Argus. The concave ice surface, modified by bed topography, extends clear to Dome Argus for $c = 2$ in Equation (7) during gravitational collapse. The ungrounded region extends to the fjord headwall where a bedrock hill (or sill) has produced a local ice dome. The ungrounded region has expanded far inland when gravitational collapse is nearly complete for $c = 0.1$, and the local ice dome has become an ice rise on a "captured" ice shelf that grounds at $x \approx 400$ km. Erlingsson (2006, 2008) discusses "captured" ice shelves.

Panel 5 in Figure 7 shows gravitational collapse along flowline five, which enters Support Force Glacier today with $h_O = 825$ m at $x = 0$ and ϕ decreasing from 1.0 to 0.5 in the fjord before rising to 0.6 on a bedrock hill (or sill) at $x = 250$ km, then falling to 0.3 clear to Dome Argus on a bed close to sea level until $x = 850$ km. The ice surface is convex the whole way today, but becomes concave most of the way when $c = 2$ in Equation (7), during gravitational collapse. Stream flow probably passes around the local ice dome at $x = 250$ km. When gravitational collapse is nearly complete at $c = 0.1$, the nearly flat ice surface from $x = 300$ km to $x = 800$ km is a "captured" ice shelf. If the grounding line were able to cross over the bedrock sill of the Transantarctic Mountains, a calving bay might be able to migrate up a stagnant Support Force Glacier and discerp ice over the submarine basins in Figure 6. This happened during the last deglaciation when a calving bay migrated up an ice stream in Hudson Strait and caved out the central accumulation zone of the Laurentide Ice Sheet (Hughes et al., 1977).

Figures 8 and 9 show ice surface elevation contours in the map plane for $c = 2.0$ and $c = 0.1$ in Equation (7) during and after gravitational collapse based on the flowline surface profiles in Figure 7. Areas of the bed below sea level are dotted. These figures were produced by drawing contour lines that connect points of equal ice elevations along flowlines in Figure 7, shown as dashed lines in Figures 8 and 9. Note the change in the flow pattern during collapse, seen where dashed lines are no longer normal to ice elevation contour lines. Figure 8 shows a state of gravitational collapse comparable to conditions today in the Amery ice drainage system. Institute Ice Stream, Mercer Ice Stream, and East Antarctic outlet glaciers south of Byrd Glacier discharge ice from a local ice ridge behind the Transantarctic Mountains. This should reduce ice entering Ross Ice Shelf, throwing it into a strongly negative mass balance that exposes it to catastrophic disintegration. The ice ridge was produced by extensive downdraw of ice discharged by Foundation Ice Stream and Support Force Glacier, both of which are grounded far below sea level, and

https://doi.org/10.1016/j.yqres.2010.12.001 Published online by Cambridge University Press

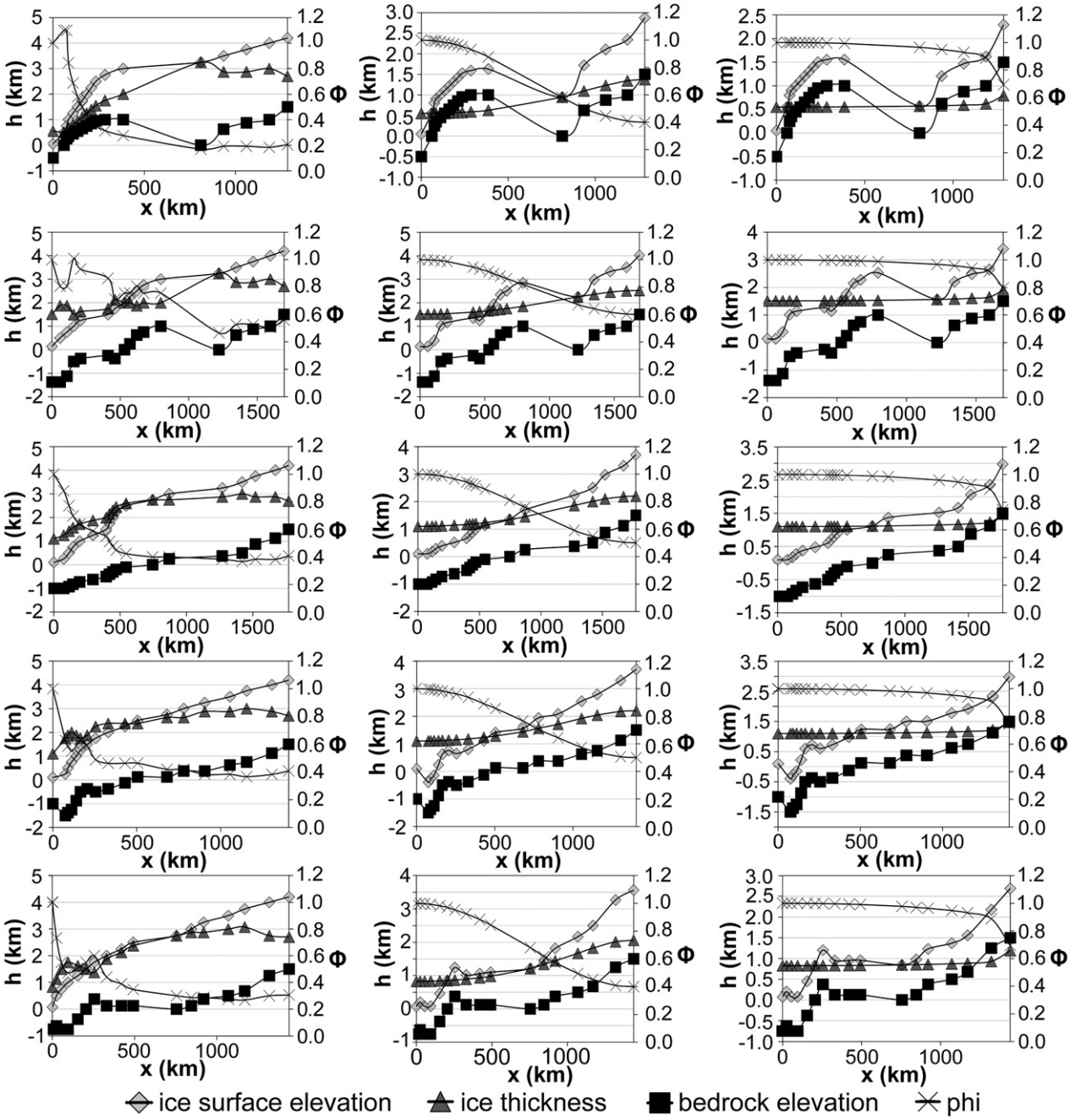

Figure 7. Surface, bed, and ice thickness profiles, and φ variations from Eq. (6), along the five flowlines in Fig. 6 at present (left), during gravitational collapse at c = 2.0 (center), and after gravitational collapse at c = 0.1 (right), using c in Eq. (7). Plots from top to bottom are for respective flowlines 1 through 5, showing ϕ variations in left-to-right panels for each flowline.

therefore subjected to the Thomas (1977) marine ice instability after the West Antarctic Ice Sheet has collapsed. Dome Argus remains 4000 m high, as it is today, but the area of East Antarctic ice discharged through bottleneck ice streams has doubled.

Figure 9 shows a final stage of collapse for which ice-bed decoupling is nearly complete all the way to Dome Argus, which has lowered 250 m. The bottleneck ice drainage basin is greatly expanded, now capturing much of the ice formerly discharged into Filchner Ice Shelf by East Antarctic outlet glaciers draining Queen Maud Land, making this ice shelf vulnerable to catastrophic disintegration. Collapse is most complete below 1500 m of ice elevation and over a bed largely below sea level. Ice at an elevation of 1000 m over a broad area is behaving like a vast interior ice shelf, a "captured ice shelf" as discussed by Erlingsson (2006, 2008) for ice floating over Subglacial Lake Vostok in East Antarctica today at Russia's Vostok Station, and formerly under parts of the Laurentide Ice Sheet. Once captured ice shelves find an outlet to the sea, they can be discerped by calving bays. This process carved out the heart of the Laurentide Ice Sheet in less than 200 years (Hughes et al., 1977).

Possible contributions of East Antarctic ice to global sea level

Sea level rises associated with collapse of the Amery and bottleneck ice drainage systems are based on estimates of the average ice thickness lost during collapse, areas of the ice drainage systems, and present-day ocean surface area. For each ice drainage system, the average ice thickness lost during collapse was calculated based on the before-and-after differences in ice elevation at each major contour

https://doi.org/10.1016/j.yqres.2010.12.001 Published online by Cambridge University Press

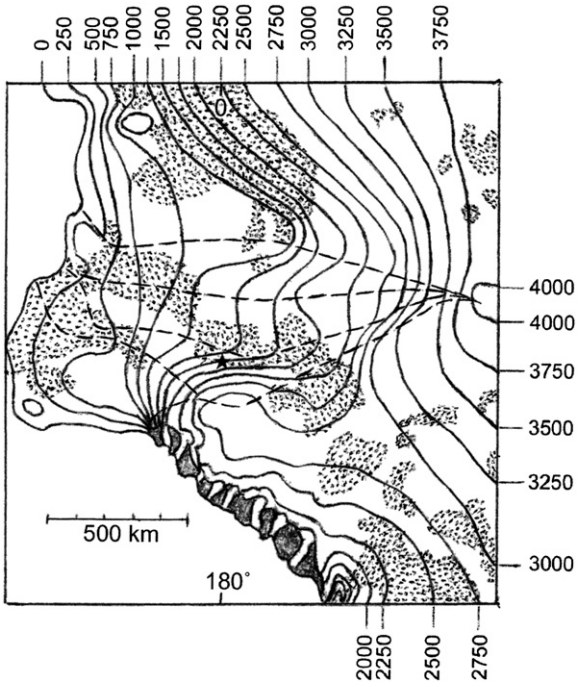

Figure 8. Ice surface elevation contours at 250 m intervals for the Bottleneck ice drainage system using flowlines in Fig. 6 and ϕ values for c = 2.0 in Eq. (7) during gravitational collapse. Dotted areas are below sea level, see Fig. 6. The black star locates the South Pole. Ice elevations in meters are given where elevation contour lines meet the edges of the figure.

line connecting the flowlines, using Amery Figure 2, and bottleneck Figure 7. For each flowline, the total ice loss was determined and, from these totals, an average ice loss was calculated for the drainage system, representative of the average ice loss along any flowline within the system. This average ice loss was then multiplied by the

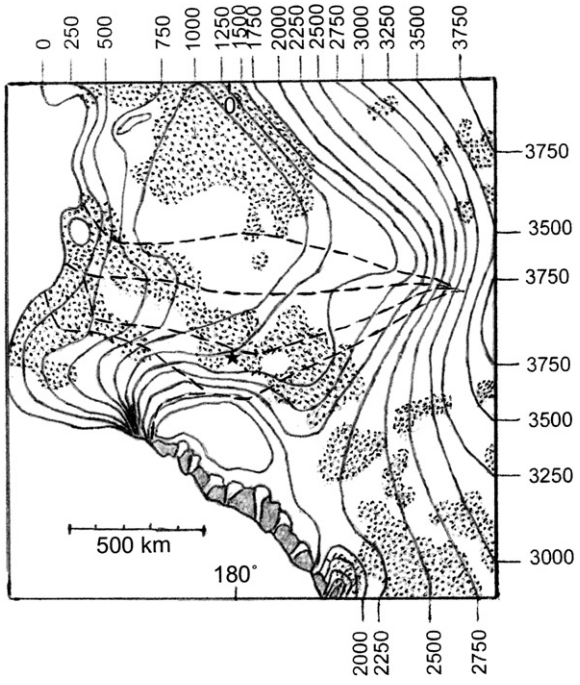

Figure 9. Ice surface elevation contours at 250 m intervals for the Bottleneck ice drainage system using flowlines in Fig. 6 and ϕ values for c = 0.1 in Eq. (7) during gravitational collapse. Dotted areas are below sea level, see Fig. 6. The black star locates the South Pole. Ice elevations in meters are given where elevation contour lines meet the edges of the figure.

area of the ice drainage system to determine the total volume of ice lost for the entire system. Enlargement of the bottleneck system, compare Figures 6 and 9, was included in this approximation. After converting this ice volume to water equivalence, the loss of water volume was divided by the present-day area of the ocean surface to obtain the resulting sea-level rise due to collapse. The resulting rise in sea level, with no correction for isostatic adjustments in this approximation, is approximately 2.3 m and 4.7 m in the respective Amery and bottleneck ice drainage systems. This compares with 3.3 m obtained by Bamber et al. (2009) for the remaining grounded West Antarctic Ice Sheet today. These resulting rises in sea level are, therefore, first-order estimates but nevertheless provide an initial determination of the resulting sea-level changes associated with collapse of the Amery and bottleneck ice drainage systems.

It appears that the Eemian sea level, 6 m above present sea level, could be provided by total collapse of the WAIS and partial collapse of the bottleneck drainage systems. In addition, future total collapse of the WAIS that triggered substantial collapse of the EAIS via the bottleneck might cause an accompanying 8 m future rise in sea level.

Discussion

Bell (2006) contends that "East Antarctica is an ice sheet controlled by lakes and mountains." Indeed, as deep radar sounding and precision surface altimetry encompass ever more of the EAIS, the prevalence of subglacial lakes is revealed as a striking feature of basal conditions for both the EAIS and the WAIS (eg., Robin et al., 1970; Oswald and Robin, 1973; Siegert et al., 1996; Smith et al., 2009). Many of these lakes, and possible lakes not yet discovered, are generated by ice-sheet models in the map plane that include subglacial hydrology, pioneered by Johnson (2002), but computational limitations hinder applications (e.g., Bahr, 2009; Morland, 2009a,b). A recent breakthrough is a numerical solution of the full equilibrium/momentum equations that permits three-dimensional simulation of transitions from sheet to stream to shelf flow in the Antarctic Ice Sheet (Sargent, 2009). Control for the next generation of ice-sheet models can now be provided by new advances in mapping basal conditions, notably topography and hydrology, in the map plane using synthetic aperture radar (Paden, et al., 2010). Despite limitations, three-dimensional and time-dependent ice sheet models compute basal melting and freezing rates so they can in principle calculate something like a "floating fraction" of ice, ϕ in Equation (5). For now, the physical meaning of ϕ is unclear. Does it represent the fraction of a given basal area in which small bedrock bumps of the size that "controls" basal sliding in a sliding "law" of the Weertman (1957b) type are drowned, the fraction of subglacial topography that is submerged, the fraction of basal till or sediments that becomes supersaturated and therefore loses cohesion, or combinations of these? We don't know.

What we do know is something like a floating fraction is needed to convert fully grounded sheet flow into fully floating shelf flow, and this conversion typically occurs along ice streams (Schoof and Hindmarsh, 2010). It has been known for 40 years that subglacial lakes are common beneath ice streams (e.g., Robin et al., 1970; Fricker and Scambos, 2009), so these are places where ice-bed uncoupling is complete. Moreover, these lakes are often interconnected and dynamic, with the ability to fill and drain rapidly (Stearns et al., 2008; Fricker and Scambos, 2009; Smith et al., 2009), and this activity can be modeled (Johnson, 2002).

Byrd Glacier has the largest ice drainage system in Antarctica, see Figure 1. Two large subglacial lakes have been discovered in the zone of strongly converging flow, just beyond its fjord headwall, and recent drainage of these lakes coincides with a substantial velocity increase of Byrd Glacier (Stearns et al., 2008). This result would not have been predicted from initial attempts to model Byrd Glacier by Whillans et al. (1989) and Scofield et al. (1991), studies which concluded the bed was largely frozen. Observations by Stearns et al. (2008) are

https://doi.org/10.1016/j.yqres.2010.12.001 Published online by Cambridge University Press

predictable from the geometrical approach that includes "floating fraction" ϕ as the controlling variable. In an application that combines the geometrical force balance with the conventional mass balance, ϕ values are produced that decrease from 1.0 at the ungrounding line of Byrd Glacier in an uneven way to 0.4 in front of the fjord headwall, and then increases to 0.6 just beyond the headwall where the two subglacial lakes are located (Reusch and Hughes, 2003). These results hold, with somewhat lower ϕ values, 0.5 beyond the headwall for example, using Equation (6) obtained from just the geometrical force balance (Hughes, 2009b). Both results are wholly compatible with the behavior reported by Stearns et al. (2008). They suggest that the lakes found an outlet at a low point eroded on the headwall, and the discharged lake water increased ice-bed uncoupling under Byrd Glacier, allowing its velocity to increase.

As a note of caution, ice thickness h_O in Equation (6) is poorly known for many East Antarctic ice streams, including those studied here. Where direct measurements are lacking or conflicting, the only alternative is using precision surface altimetry and the buoyancy requirement for floating ice. Even here, ice and water densities are not known with sufficient accuracy. Equation (5) is the defining equation for floating fraction ϕ, but Equation (6) is the working equation, in which h_O at $x=0$ replaces h_F at $x>0$ along flowlines. Because it is our working equation, Equation (6) is derived in the Appendix.

A feature of Equation (6) is that it requires hydraulic continuity so $\phi>0$ when $h_O>0$. Then water flows from sources to sinks at all points within the ice drainage system for any ice stream, even if the ice flow regime changes over time. Therefore Equation (6), our working equation, can be used to compute h_I for specified ϕ, or vice versa, at all points within the ice drainage system in Figures 8 and 9 during and after gravitational collapse. The only requirement is that h_O remains known for each ice stream. That requirement is met by keeping the ice-stream ungrounding lines anchored to bedrock sills along the Transantarctic Mountains during gravitational collapse. That said, Equation (5), the defining equation, is better. It allows $\phi=0$ for fully grounded ice on thawed and frozen beds even when $h_O>0$, a common condition, see Hughes (1998, Chapter 3) and Wilch and Hughes (2000) for the Antarctic Ice Sheet. Including the mass balance with the force balance allows Equation (5) to also be the working equation (Hughes, 1998, Chapters 3 and 6). The downside is the resulting ϕ equation loses simplicity.

Conclusions

Two conclusions follow from our study. First, it should no longer be assumed that the EAIS is inherently stable. The EAIS seems to be the most likely source for half of the higher Eemian sea level (WAIS collapse provided the other half), and if it partly collapsed during that most recent interglacial, it can partly collapse during the present interglaciation. Second, modeling the dynamics of ice sheets needs to include something akin to a "floating fraction" of ice that can change rapidly in both space and time. These models would treat both ice dynamics and subglacial hydrology in the map plane and could then assess postulate (3) of our hypothesis: that because of postulates (1) and (2), ice sheets can rapidly collapse and disintegrate, thereby removing ice sheets from Earth's climate system and forcing abrupt climate change.

Acknowledgments

This study was the final examination in a course, The Role of Continental Glaciers in Climate Change, taught at the University of Maine. James Fastook provided the surface and bed topographic maps in Figures 2 and 6 from BEDMAP data. Beverly Hughes prepared the manuscript for publication. Eric Steig and Alan Gillespie were invaluable in making our work acceptable for publication. The U.S. National Science Foundation, through the Center for Remote Sensing of Ice Sheets (CReSIS) at the University of Kansas, supported the work.

Appendix A. Derivation of Equation (6)

Figure A1 shows conditions along a flowband for which Equation (6) was derived. Here $P_I=\rho_I\, g\, h_I$ is basal ice pressure for ice of density ρ_I and height h_I subject to gravity acceleration g, x is horizontal distance upslope along the flowband with $x=0$ at its ungrounding line, and $\sigma_F=\overline{P}_I\phi^2$ for $\overline{P}=\frac{1}{2}\, P_I$ is a longitudinal "flotation" stress that exists in regions of the flowband for which ice is uncoupled from the bed due to floating fraction ϕ linked to floating width w_F less than flowband width w_I and "effective" floating height h_F in Figure A1 as follows:

$$\phi=\frac{w_F}{w_I}=\frac{h_F}{h_I}=\frac{h_W(\rho_W/\rho_I)}{h_I}=\frac{\rho_W g h_W}{\rho_I g h_I}=\frac{P_W}{P_I} \tag{A1}$$

Here ρ_W is water density and $P_W=\rho_W\, g\, h_W$ is an "effective" basal water pressure linked to "effective" water height h_W that acts as a proxy for w_F, since ice of height $h_F=h_W\,(\rho_W/\rho_I)$ floats in water of height h_W. The actual basal water pressure is close to P_I, differing only when basal water flows from sources to sinks. Resistance to basal sliding in grounded width $w_I - w_F$ gives rise to P_W as an "effective" basal water pressure that resists downstream ice flow.

In Figure A1 (bottom), triangular areas $1+2+3+4$ and $5+6+7+8$ represent longitudinal gravitational forcing respectively at x and $x+\Delta x$. Basal shear stress τ_O and side shear stress τ_S that resist gravitational flow are linked to respective changes in area 5–1 and 6–2 in incremental length Δx as $\Delta x\to 0$.

As a practical matter in calculating ϕ from Equation (6), flowline profiles are often obtained by aerial radar sounding along flightlines down centerlines of ice streams where side shear stresses vanish. Hughes (2009b) obtained Equation (6) for ice flowbands having width w_I of ice streams along which both basal shear stress τ_O and side shear stress τ_S are linked to ϕ, where τ_O and τ_S are linked to changes in respective areas *ABG* and *BEFG* along Δx as $\Delta x\to 0$ in Figure A2, which are areas 1 and 2 in Figure A1. Because side shear exists along ice streams, but vanishes along their centerlines, ice elevations along centerlines will be increased by side shear.

This can be taken into account by using an "effective" basal shear stress τ_O^* that exceeds τ_O along centerlines where τ_S vanishes and τ_O^* is linked to the change in area *ABEF* in Figure A2, thereby increasing the change in gravitational driving force ΔF_G to "effective" force ΔF_G^* obtained from Figure A2:

$$\begin{aligned}\Delta F_G^* &= (A'\,B'\,E'\,F'-ABEF)=\Delta(ABEF)=\Delta(ABG+BEFG)\\ &=\Delta\left[\tfrac{1}{2}\rho_I g h_I^2(1-\phi)^2+\rho_I g h_I^2\phi(1-\phi)\right]=\Delta\left[\tfrac{1}{2}\rho_I g h_I^2\phi\left(1-\phi^2\right)\right]\\ &=\rho_I g h_I\left[\left(1-\phi^2\right)\Delta h_I-h_I\phi\Delta\phi\right]\end{aligned} \tag{A3}$$

where triangle *ABG* has basal pressure $\rho_I\, g\,(h_I - h_F)=\rho_I\, g\, h_I\,(1\text{-}\phi)$ and height $h_I - h_F=h_I\,(1-\phi)$, and parallelogram *BEFG* has basal pressure $\rho_I\, g\,(h_I - h_F)=\rho_I\, g\, h_I\,(1-\phi)$ and height $h_F=h_I\,\phi$. Equation (A3) balances the change in "effective" centerline resisting force ΔF_R^* given by:

$$\Delta F_R^*=\tau_O^*\Delta x \tag{A4}$$

https://doi.org/10.1016/j.yqres.2010.12.001 Published online by Cambridge University Press

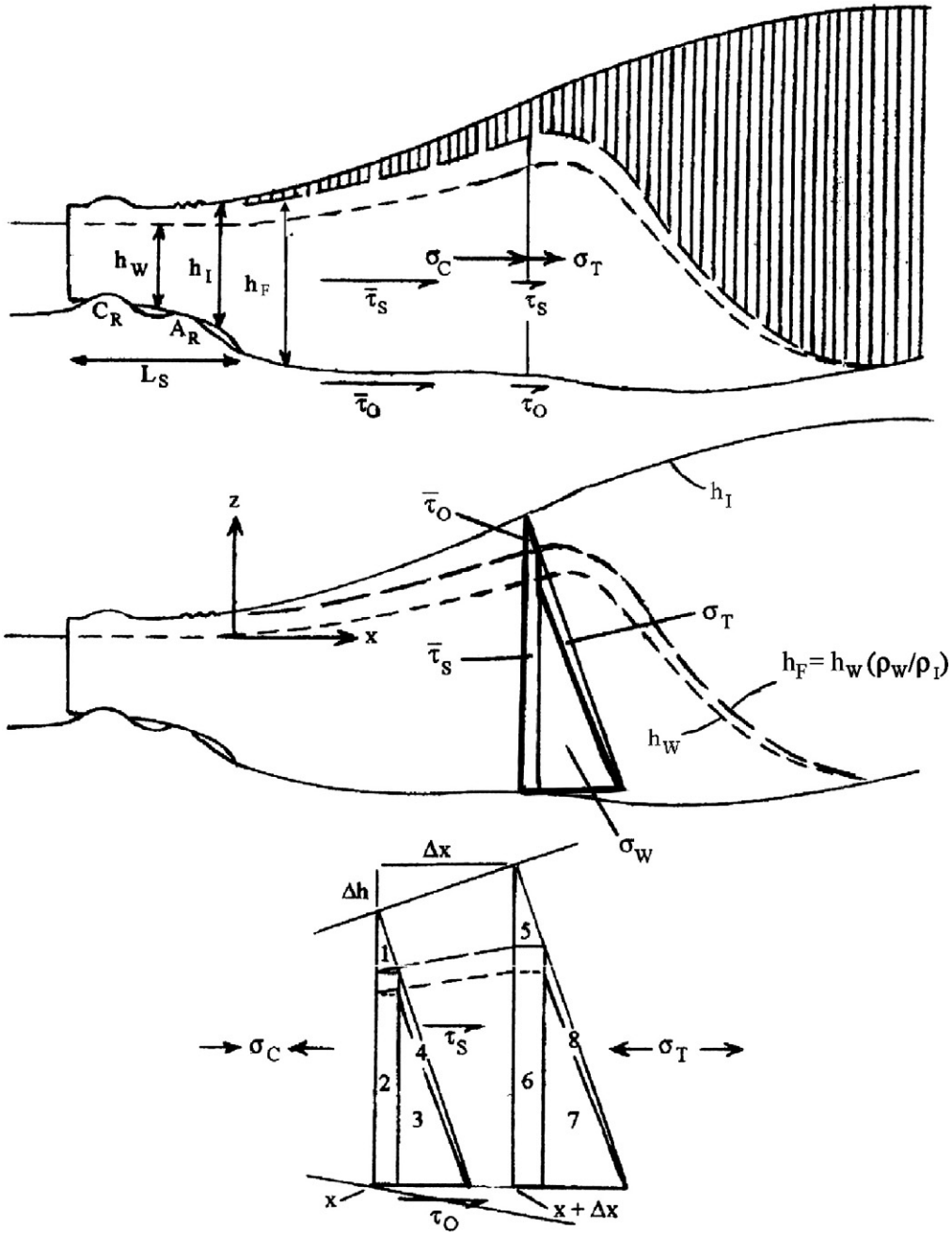

Figure A1. The geometrical force balance on an ice stream ending as a confined ice shelf. Top: 98 Kinematic stresses that resist gravitational flow. The bed supports ice in the shaded area. Ice in 99 the unshaded area is supported by basal water pressure. Middle: Gravitational forces at x 100 represented as triangles and a rectangle are linked to specific kinematic stresses. The area inside 101 the thick border is linked to σC. Heights hI, hW, and hF are measured from the bed for x > 0. 102 Bottom: Kinematic stresses and gravitational forces along Δx. Kinematic and gravitational forces 103 are balanced along x and Δx.

Equating Equations (A3) and (A4), setting $P_I = \rho_I g\, h_I$, and $\Delta h_I = \Delta h$ on horizontal "steps" for an up-down "staircase" bed so $\Delta h/\Delta x \to \alpha$ and $\Delta\phi/\Delta x \to \partial\phi/\partial x$ when $\Delta x \to 0$, then:

$$\tau_O^* = P_I\left[\left(1-\phi^2\right)\alpha - h_I\phi(\partial\phi/\partial x)\right] \tag{A5}$$

Equation (A5) applies at distance x along a flowline upstream from where ice becomes afloat at $x = 0$. Elimination of τ_S eliminates side shear along grounded ice-shelf side lengths L_S and ice-rise circumference CR in Figure A1. Area A_R of ice rumples is replaced with longitudinal diameter D_R. Balance mean basal shear force $\overline{\tau}_O^*\,(x + D_R)$ against gravitational forcing linked to area $ABEF$:

$$\overline{\tau}_O^*(x + D_R) = ABEF = ABG + BEFG = {}^1\!/_2\,\rho_I g h_I^2(1-\phi)^2 + \rho_I g h_I^2\phi(1-\phi)$$
$$= {}^1\!/_2\,\rho_I g h_I^2\left(1-\phi^2\right) = \overline{P}_I h_I\left(1-\phi^2\right) \tag{A6}$$

Solving Equation (A6) for $\overline{\tau}_O^*$ gives:

$$\overline{\tau}_O^* = \overline{P}_I h_I\left(1-\phi^2\right)/(x + D_R) \tag{A7}$$

https://doi.org/10.1016/j.yqres.2010.12.001 Published online by Cambridge University Press

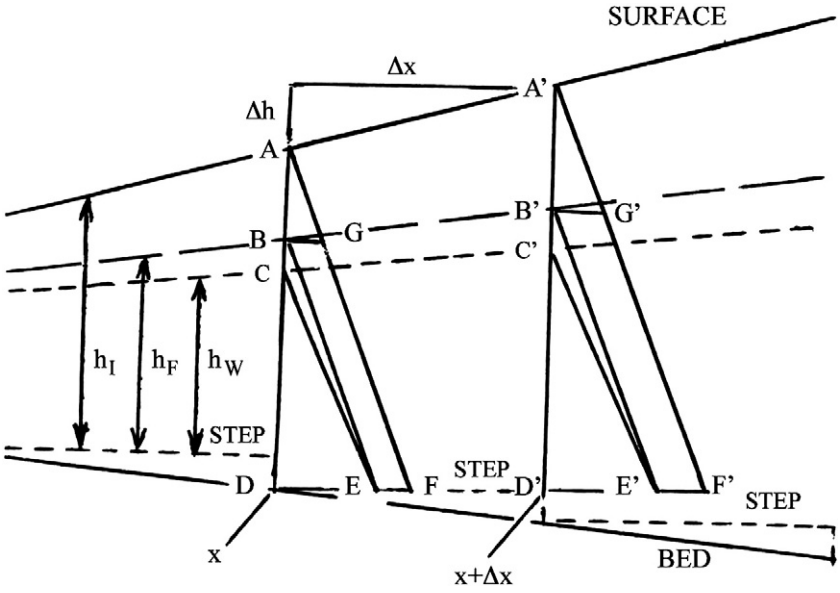

Figure A2. Gravitational forces at x and at x + Δx represented geometrically.

Tensile stress σ_T "pulls" upstream ice and compressive stress σ_C "pushes" downstream ice at x in Figure A1. The downstream compressive force is then:

$$\sigma_C h_I = \overline{\tau}^*_O(x + D_R) + (\overline{P}_W h_W)_O = \overline{P}_I h_I\left(1-\phi^2\right) + (\overline{P}_I h_O)(\rho_I/\rho_W)$$
$$= {}^1\!/_2\,\rho_I g h_I^2\left(1-\phi^2\right) + {}^1\!/_2\,\rho_I g h_O^2(\rho_I/\rho_W) \quad \text{(A8)}$$

Here Equation (A7) is substituted for $\overline{\tau}^*_O$ and compressive water force $(\overline{P}_W\ h_W)_O$ is at $x=0$ where $h_I=h_O$, $\overline{P}_W=\overline{P}_I=1\ /\ 2\rho_I g h_O$ and $h_W=h_O\ (\rho_I/\rho_W)$. Tensile force $\sigma_T\ h_I$ at x is linked to area 4 = area (3 + 4) – area 3 in Figure A1:

$$\sigma_T h_I = {}^1\!/_2\,\rho_I g h_F^2 - {}^1\!/_2\,\rho_I g h_F h_W = {}^1\!/_2\,\rho_I g h_I^2(1-\rho_I/\rho_W)\phi^2 \quad \text{(A9)}$$
$$= \overline{P}_I h_I(1-\rho_I/\rho_W)\phi^2$$

Gravitational driving force $\overline{P}_I h_I$ at x is resisted by $\sigma_C\ h_I + \sigma_T\ h_I$ such that, using Equation (A9):

$$\sigma_C h_I = \overline{P}_I h_I - \sigma_T h_I = \overline{P}_I h_I - \overline{P}_I h_I(1-\rho_I/\rho_W)\phi^2 \quad \text{(A10)}$$
$$= {}^1\!/_2\,\rho_I g h_I^2\left[1-(1-\rho_I/\rho_W)\phi^2\right]$$

Equating Equations (A8) and (A10):

$$h_I^2\left(1-\phi^2\right) + h_O^2(\rho_I/\rho_W) = h_I^2\left[1-(1-\rho_I/\rho_W)\phi^2\right]$$

Solving for ϕ variations along the flowline gives:

$$\phi = h_O/h_I \quad \text{(A11)}$$

Equation (A11) along flowlines is identical with Equation (6) along flowbands, making this first approximation of ϕ variations for ice-stream centerlines and widths both simple and robust.

References

Alley, R.B., Bindschadler, R.A., 2001. The West Antarctic ice sheet: behavior and environment. American Geophysical Union (Antarctic Research Series), Washington, DC. 296 pages.

Alley, R.B., Gow, A.J., Meese, D.A., Waddington, E., Bolzan, J., 1997. Grain-scale processses, folding, and stratigraphic disturbance in the GISP2 ice core. Journal of Geophysical Research 102 (26), 819–826 830.

Bahr, D., 2009. On fundamental limits to glacier flow models: computational theory and implications. Journal of Glaciology 55, 229–238.

Bamber, J.L., Riva, R.E.M., Vermeersen, B.L.A., LeBrocq, A.M., 2009. Reassessment of the potential sea-level rise from a collapse of the West Antarctic ice sheet. Science 324, 901–903.

Bell, R.E., 2006. East Antarctica: an ice sheet controlled by lakes and mountains. Lecture deliviered on 1 November 2006 at the Center for Remote Sensing Ice Sheets (CReSIS), University of Kansas.

Bindschadler, R.A., 1997. Actively surging West Antarctic ice streams and their response characteristics. Annals of Glaciology 24, 409–413.

Christoffersen, P., et al., 2008. Warm Atlantic water drives Greenland Ice Sheet discharge-dynamics. [Abstract C31B-501] EOS **89,** Fall Meeting Supplement.

Craven, M., Allison, I., Fricker, H.A., Warner, R., 2009. Properties of a marine ice layer under the Amery Ice Shelf, East Antarctica. Journal of Glaciology 55, 717–728.

Denton, G.H., Hughes, T.J., 2002. Reconstructing the Antarctic ice sheet at the last glacial maximum. Quaternary Sciences Reviews 21, 193–202.

Drewry, D.J., ed. 1983. Antarctica: Glaciological and Geophysical Folio. Scott Polar Research Institute, University of Cambridge, Cambridge, UK.

Erlingsson, U., 2006. Lake Vostok behaves like a 'captured lake' and may be near to creating an Antarctic Jökulhlaup. Geografiska Annaler 88A, 1–7.

Erlingsson, U., 2008. A Jökulhlaup from a Laurentian captured ice shelf to the gulf of Mexico could have caused the bolling warming. Geografiska Annaler 90A, 125–140.

Fricker, H.A., Scambos, T.A., 2009. Connected subglacial lake activity on lower Mercer and Whillans Ice Streams, West Antarctica, 2003–2008. Journal of Glaciology 55, 303–315.

Hall, B.L., Baroni, C., Denton, G.H., 2004. Holocene relative sea-level history of the southern Victoria Land coast, Antarctica. Global and Planetary Change 42, 241–263.

Hofstede, C. M. 2008. "Ice Stream Dynamics: A Transition Between Sheet Flow and Shelf Flow." Ph.D. thesis, University of Maine.

Holland, D.M., Thomas, R.H., de Young, B., Ribergaard, M.H., Lyberth, B., 2008. Acceleration of Jakobdshavn Isbrae triggered by warm subsurface ocean waters. Nature Geoscience 1, 659–664.

Hollin, J., 1962. On the glacial history of Antarctica. Journal of Glaciology 4, 173–195.

Hollin, J.T., 1972. Interglacial climates and Antarctic ice surges. Quaternary Research 2, 401–408.

Hughes, T., 1973. Is the West Antarctic ice sheet disintegrating? Journal of Geophysical Research 78, 7884–7910.

Hughes, T., 1975. The West Antarctic ice sheet: instability, disintegration, and initiation of ice ages. Reviews of Geophysics and Space Physics 13, 502–526.

Hughes, T., 1981. The weak underbelly of the West Antarctic ice sheet (letter). Journal of Glaciology 27, 518–525.

Hughes, T., 1998. Ice Sheets. Oxford University Press, New York. 343 pages.

Hughes, T., 2004. Greenland ice sheet and rising sea level in a worst-case climatic change scenario. Polar Meteorology and Glaciology 18, 54–71.

Hughes, T., 2009a. Modeling ice sheets from the bottom up. Quaternary Science Reviews 28, 1831–1849.

Hughes, T., 2009b. Variations in ice-bed coupling beneath and beyond ice streams: the force balance. Journal of Geophysical Research 114, 20 pp.

Hughes, T.J., Denton, G.H., Grosswald, M.G., 1977. Was there a late Würm Arctic ice sheet? Nature 266, 596–602.

Johnson, J. 2002. "A Basal Water Model for Ice Sheets." Ph.D. thesis, University of Maine.

https://doi.org/10.1016/j.yqres.2010.12.001 Published online by Cambridge University Press

Joughin, I.R., Tulaczyk, S.M., Bamber, J.L., Blankenship, D.D., Holt, J.W., Scambos, T.A., Vaughan, D.G., 2009. Basal conditions for Pine Island and Thwaites Glalciers, West Antarctica, determined using satellite and airborne data. Journal of Glaciology 55, 245–257.
Kamb, B., Raymond, C.F., Harrison, W.D., Engelhardt, H., Brugman, M.M., Pfeffer, T., 1985. Glacier surge mechanism: 1982–1983 surge of Variegated Glacier, Alaska. Science 227, 469–479.
Kellogg, T.B., Kellogg, D.E., 1987. Recent glacial history and rapid ice-stream retreat in the Amundsen Sea. Journal of Geophysical Research 92, 8859–8864.
Mayewski, P.A., Meeker, L.D., Twickler, M.S., Whitlow, S., Yang, Q., Prentice, M., 1997. Major features and forcing of high latitude Northern Hemisphere Atmospheric Circulation using a 110,000 year long glaciochemical series. Journal of Geophysical Research (Special Issue-Oceans/Atmosphere) 102 (26) 345-26, 366.
Mercer, J.H., 1968. Antarctic ice and Sangamon sea level. International Association of Scientific Hyrdrology 79, 217–225 Publication Number.
Mercer, J.H., 1970. A former ice sheet in the Arctic Ocean. Palaeogeography, Palaeoclimatology, Palaeoecology 8, 19–27.
Morland, L.W., 2009a. Primary, secondary and teriary creep of ice modelled as a viscoelastic fluid. Journal of Glaciology 55, 170–178.
Morland, L.W., 2009b. Age-depth correlation, grain growth and dislocation-density evolution, for three ice cores. Journal of Glaciology 55, 345–352.
Nye, J.F., 1952. The mechanics of glacier flow. Journal of Glaciology 2, 82–93.
Oswald, G.K.A., Robin, G.deQ., 1973. Lakes beneath the Antarctic ice sheet. Nature 245, 251–254.
Paden, J., Akins, T., Dunson, D., Allen, C., Gogineni, P., 2010. Ice-sheet bed 3-D tomography. Journal of Glaciology 56, 3–11.
Paterson, W.S.B., 1994. The Physics of Glaciers, 3rd Edition. Butterworth-Heineman, Oxford, U.K. 481 pages.
Pfeffer, W.T., Hasrper, J.T., O'Neel, S., 2008. Kinematic constraints on glacier contributions to 21st-century sea-level rise. Science 321, 1340–1343.
Reusch, D., Hughes, T.J., 2003. Surface "waves" on Byrd Glacier. Antarctic Science 16, 547–555.
Robin, G.deQ., Weertman, J., 1973. Cyclic surging of glaciers. Journal of Glaciology 12, 3–18.
Robin, G.deQ., Swithinbank, C.W.M., Smith, B.M.E., 1970. Radio-echo exploration of the Antarctic ice sheet. International Association of Scientific Hydrology 86, 97–115.
Sargent, A. 2009. "Modeling Ice Streams." Ph. D. thesis, University of Maine.
Schoof, C., 2007. Ice sheet grounding line dynamics: steady states, stability and hysteresis. Journal of Geophysical Research, Earth Surface 112, F03S28.
Schoof, C., Hindmarsh, R.C.A., 2010. Thin-film flows with wall slip: an asymptotic analysis of higher order glacier flow models. Quaternary Journal of Mechanics and Applied Mathematics 63 (1), 73–114, doi:10.1093/qjmam/hbp025.
Scofield, J.P., Fastook, J.L., Hughes, T., 1991. Evidence for a frozen bed, Byrd Glacier, Antarctica. Journal of Geophysical Research 96 (11) 649-11,655.
Siegert, M.J., Dowdeswell, J.A., Gorman, M.R., McIntyre, N.F., 1996. An inventory of Antarctic subglacial lakes. Antarctic Science 8, 281–286.
Smith, B.E., Fricker, H.A., Joughin, I.R., Tulaczyk, S.M., 2009. An inventory of active subglacial lakes in Antarctica detected by ICESat (2003–2008). Journal of Glaciology 55, 573–595.
Stearns, L.A., Smith, B.E., Hamilton, G.S., 2008. Increased flow speed on a large East Antarctic outlet glacier due to subglacial floods. Nature Geoscience 1, 827–831.
Stuiver, M., Denton, G.H., Hughes, T.J., Fastook, J.L., 1981. History of the marine ice sheet in West Antarctica during the last glaciation: a working hypothesis. In: Denton, G.H., Hughes, T.J. (Eds.), The Last Great Ice Sheets. Wiley-Interscience, New York, pp. 319–436.
Thomas, R.H., 1973a. The creep of ice shelves: theory. Journal of Glaciology 12 (64), 45–53.
Thomas, R.H., 1973b. The creep of ice shelves: interpretation of observed behavior. Journal of Glaciology 12, 55–70.
Thomas, R.H., 1977. Calving bay dynamics and ice sheet retreat up the St. Lawrence valley system. Géographie Physique et Quaternaire 31, 347–356.
Thomas, R.H., 2004. Force-perturbation analysis of recent thinning and acceleration of Jakobshavns Isbrae, Greenland. Journal of Glaciology 50, 57–66.
Thomas, R.H., Bentley, C.R., 1978. A model for Holocene retreat of the West Antarctic ice sheet. Quaternary Research 10, 150–170.
Thomas, R.H., Frederick, E.B., Krabill, W.B., Manizade, S., Martin, C., 2009. Recent changes on Greenland outlet glaciers. Journal of Glaciology 55, 147–162.
Van der Wal, R.S.W., et al., 2008. Large and rapid melt-induced velocity changes in the ablation zone of the Greenland ice sheet. Science 321, 111–113.
Weertman, J., 1957a. Deformation of floating ice shelves. Journal of Glaciology 3, 38–42.
Weertman, J., 1957b. On the sliding of glaciers. Journal of Glaciology 3, 33–38.
Weertman, J., 1974. Stability of the junction of an ice sheet and an ice shelf. Journal of Glaciology 13, 3–11.
Whillans, I.M., Chen, Y.H., van der Veen, C.J., Hughes, T., 1989. Force budget III: Application to three-dimensional flow of Byrd Glacier, Antarctica. Journal of Glaciology 35, 68–80.
Wilch, E., Hughes, T., 2000. Mapping basal thermal zones beneath the Antarctic ice sheet. Journal of Glaciology 46 (153), 297–310.